Desalination and Water Treatment
www.deswater.com

doi: 10.5004/dwt.2021.26590

210 (2021) 340–350
January

Adsorption of lead from aqueous solution by chitosan/rectorite composite sponge

Tao Feng[a,b,*], Shuai Wang[a], Pengwei Li[a], Yimin Hu[a], Yu Wang[a], Jun Han[a,b]

[a]*College of Resources and Environmental Engineering, Wuhan University of Science and Technology, Wuhan 430081, China, Tel. +86 27 68862880; emails: fengtaowhu@163.com (T. Feng), 940789894@qq.com (S. Wang), 826461375@qq.com (P. Li), hymwust@163.com (Y. Hu), yuwang@wust.edu.cn (Y. Wang), hanjun@wust.edu.cn (J. Han)*
[b]*Hubei Key Laboratory for Efficient Utilization and Agglomeration of Metallurgic Mineral Resources, Wuhan University of Science and Technology, Wuhan 430081 China*

Received 15 November 2019; Accepted 19 September 2020

ABSTRACT

Rectorite/chitosan (REC/CS) and cross-linked CS composite sponge was prepared by freeze-drying method and characterized by Fourier-transform infrared spectroscopy, scanning electron microscopy and X-ray diffraction. The REC/CS sponge possessed interconnected three-dimensional macropores with pore sizes of 30–100 μm. REC/CS composite sponge was employed as adsorbents for the removal of Pb^{2+} from aqueous solutions in a batch system. The result showed that the adsorption capacity of cross-linked CS sponge and REC/CS composite sponge was 18.87 and 27.03 mg/g, respectively. Equilibrium isotherm study showed a very good fit with the Langmuir isotherm equation for the monolayer adsorption process, while the adsorption process can be well described by the second-order kinetic model. The adsorption process was determined by two steps of internal diffusion and liquid membrane diffusion, the adsorption rate of the first step was faster than the second step.

Keywords: Chitosan; Rectorite; Sponge; Adsorption; Lead

1. Introduction

With the development of industry, the problem of water pollution caused by heavy metals is becoming more and more serious. Lead has toxicity in low concentration, and is difficult to be degraded. The bioaccumulation of lead causes a serious threat to organisms and human health. Drinking the lead-bearing water for a long time, the nervous system of human could be disordered and the cardiovascular system could be injured to a lesser degree [1]. The wide application increases the emission of lead greatly, the concentration of lead in industrial wastewater reaches 200–500 mg L^{-1}, which is too high for the environment [2]. So the removal of lead from wastewater became one of the critical issues.

Nowadays, the methods of removing heavy metals from aqueous solutions include precipitation, electrochemical, biological, membrane filtration, ion exchange, adsorption, and so on [3–6]. Among the above, adsorption method is widely used due to its remarkable effect, low energy consumption, easy operation, and reusability. Therefore, adsorption has broad prospects in the treatment of heavy metals wastewater. The key factor influencing the adsorption effect is the choice of adsorbent.

Traditional adsorbent always exists in the powder or spherical form. But adsorbent with small size is easy to be drained in application, which increases the possibility of secondary pollution. Cheng et al. [7] prepared chelating sponge for adsorption of Ni(II) and Cd(II) from water samples.

* Corresponding author.

Zhao et al. [8] prepared recyclable S-doped graphene sponge for Cu^{2+} adsorption. The sponge adsorption material has become an important direction. Compared with traditional adsorbent, the sponge adsorbent is easier to be separated from water, which is beneficial for reusing and reducing the operation cost. Chitosan (CS) is obtained by deacetylation of chitin, which widely exists in various animals and plants. The existence of amino and hydroxyl groups in its structure provides a good adsorption performance for heavy metals [9,10]. At the same time, CS is prone to be chemically modified, and modification is the efficient way to widen the application of CS. As a kind of natural polymer material, CS is possible to be the raw material for preparing sponge adsorbent because of the large amount of active groups [11].

Moreover, rectorite (REC) is a kind of natural clay and an interlayer silicate mineral consisting of a regular (1:1) accumulation of mica-like layer and montmorillonite-like layer. REC has been studied for its potential applications as environmental remediation agents to remove heavy metals, due to its large surface area and high ion exchange capacity [12]. Zhang et al. [13] modified the REC by combining inorganic and organic reagents. The removal rate of Pb^{2+} by the modified REC reached 100%, and the adsorption capacity reached 8.31 mg/g. But according to the previous research, the adsorption efficiency of REC is not satisfactory.

In order to promote the adsorption property of CS and REC, an environmental-friendly sponge adsorbent material was prepared. CS was modified by compounding with REC and crosslinking, using glutaraldehyde as crosslinking agent. And the sponge was prepared by freeze-drying method. The composite sponge was characterized by X-Ray diffraction (XRD), Fourier-transform infrared spectroscopy (FTIR), scanning electron microscopy (SEM), SEM-EDS, energy-dispersive spectroscopy (EDS) mapping. Static adsorption experiments had been carried out to study the adsorption property of REC/CS composite sponge for removal of lead from aqueous solutions. The factors affecting the adsorption effect were discussed, such as the mass ratio of REC and CS, pH, contact time, initial concentration, and dosage of adsorbent. And the adsorption process was analyzed by adsorption kinetic models and isothermal adsorption models.

2. Materials and methods

2.1. Chemicals and materials

CS with a degree of deacetylation more than 90% was obtained from Zhejiang Golden-Shell Pharmaceutical Co., (Yuhuan, China). REC was purchased from Hubei Xingfa Chemicals Group Co., Ltd., (Xingshan, China). The other agents used in the experiments were of analytical grade. The water used in experiments was ultrapure water.

FD-1D-50 freezing dryer was provided by Beijing Boyikang Laboratory Instruments Co., Ltd., (Beijing, China) novAA 350 atomic absorption spectrophotometer was provided by Analytik Jena, Germany.

2.2. Preparation of REC/CS composite sponge

REC/CS composite sponge was prepared by freeze-drying as follows. In a 2% (v/v) aqueous acetic acid solution, 2.5 g pure chitosan was dissolved to prepare chitosan solution, the dissolution process takes about 4 h under the condition of stirring at 120 rpm. Varied weights of 0, 0.25, 0.3125, 0.5, 0.8333, 2.5 g REC were added to the beaker with 50 mL ultrapure water, and the beaker was put in the water bath between 50°C and 60°C. The REC suspension was prepared under stirring. Then as-prepared CS solution was slowly added into the REC suspension, kept stirring for 10 h under the same condition. Crosslinking agent (2.5% [V/V] glutaraldehyde solution) was added into the mixer, and cooled to room temperature. The crosslinking reaction spent 2 h at room temperature with stirring. When the reaction was finished, the mixer was poured into several plastic culture dishes averagely. Plastic culture dishes with mixer were put in refrigerator for precooling, and then put them in freeze-dryer until totally dried. The obtained material was soaked in 0.1 mol/L NaOH solution for 30 min, followed with washing by water until the pH was close to neutral. REC/CS composite sponge was prepared after freeze-drying again.

2.3. Characterization of REC/CS composite sponge

The samples were ground into powder, and then formed into pellets with KBr at the ratio of 1:100 (w/w). FTIR spectra were recorded with KBr pellets on Nicolet-360 FTIR spectrometer in the range of 4,000–400 cm^{-1}. The crystal structure of the samples was investigated by XRD.

The morphology of the samples was characterized by SEM. At the same time, EDS analysis and EDS mapping analysis was used to study the difference of the surface elements before and after adsorption.

2.4. Adsorption experiments

0.1 g adsorbent was added into a 100 mL conical bottle containing 50 mL Pb^{2+} solution. The conical bottle was placed in a dual multi-purpose speed oscillator (120 rpm, 303.15 K) for desired time followed by filtration. The concentration of remaining Pb^{2+} in solution was detected by atomic absorption spectrophotometer. The adsorption capacity Q (mg/g) of REC/CS composite sponge is calculated from the following equation:

$$Q = \frac{\left(C_0 - C_e\right)V}{1{,}000\ m} \tag{1}$$

In the forms, C_0 and C_e represent the concentration (mg/L) of Pb^{2+} before and after adsorption, respectively. V is the volume (L) of Pb^{2+} solution before adsorption, and m is the mass (g) of the adsorbent.

3. Results and discussion

3.1. Characterization of the sponges before adsorption

3.1.1. SEM analysis

The SEM micrographs of REC/CS composite sponge before adsorption are shown in Fig. 1. In REC/CS complex solution, the Schiff base reaction between GA and CS molecules occurred, the CS molecular chains were cross-linked and REC/CS complex wet gel was formed. Water in the gel

was replaced with gas by freeze-drying under vacuum and a 3D macroscale sponge formed with a porous structure. The REC/CS sponge possessed interconnected three-dimensional macropores with pore sizes of 30–100 μm. Moreover, most of these pores were perforated and laminated, which provided enough surface area for Pb^{2+} contacting with the adsorbent. From Fig. 1, the surface performed slightly rough, due to the addition of REC powder. And the REC powder in sponge dispensed evenly.

3.1.2. FTIR analysis

FTIR analysis is a characterization method to characterize the functional structure of materials. The FTIR spectra of the samples are shown in Fig. 2. In Fig. 2a, the N–H stretching vibration occurred at 3,444 cm^{-1}, which overlapped the O–H stretch from the carbohydrate ring. However, the vibration peak shifted to 3,365 cm^{-1} after the crosslinking; addition of crosslinking agent could increase the distance between CS chains and decrease the binding force. Fig. 2c shows the FTIR spectra of REC powder. The peak at 3,647 cm^{-1} was attributed to the bending vibration of hydrogen bond formed on hydroxyl groups in Si–OH. The wide peak at 3,446 cm^{-1} was due to the bending vibration of water and hydrogen bond between water molecules. The peaks at 701 and 548 cm^{-1} were formed by bending vibration out of plane of Si–O–Al. The bending vibration of Si–O was showed at 438–488 cm^{-1} [14–16].

The characteristic peaks of CS and REC both appeared in REC/CS composite sponge as shown in Fig. 2d. Compared with the single phase, a slight shift and weakening of these peaks over the composite sponge was observed, probably due to a weak interaction between the two substances [17]. Typically, the peak of N–H shifted to 1,558 cm^{-1} due to the negative electrical properties of the silicon oxygen tetrahedron contained in the interlayer of REC, while the $–NH_2$ group in CS had an electrostatic interaction with the negative charge sites of REC when the intercalation reaction happened [12]. Furthermore, the weakness of stretching vibration of N–H and O–H in Fig. 2d demonstrated that the crosslinking reaction mainly happened on $–NH_2$ and –OH in CS. Moreover, the peak at 3,647 cm^{-1} in Fig. 2c was also weaker, which might be due to the formation of hydrogen bonds between –OH in REC and active groups in CS.

3.1.3. XRD analysis

XRD patterns are shown in Fig. 3. The diffraction peaks appeared at $2\theta = 11.90°$ and 20.08° over CS indicated a certain crystalline region in the CS molecules (Fig. 3a), which might be resulted from the intermolecular hydrogen bonds. The addition of crosslinking agent could cause a crosslinking reaction between CS chains, and destroy the hydrogen bonding between molecules, thus decreasing the crystallinity of CS (Fig. 3b) [18]. Furthermore, the XRD peaks for REC sample in the range of 10°–70° well matched with the rectorite phase (Fig. 3c). Comparing Fig. 3d with Figs. 3a and b, the peak at about 20° diminished obviously. The change might be attributed to the relatively high crystallinity of REC. It could be seen in Fig. 3d that there was no new peak arising after the compound reaction, but the peak became wider evidently. This result was because the combination of REC and CS cannot produce a chemical reaction to form a new substance, but it affected the crystallization degree of the material. So that the crystallization degree of the rectorite was reduced, and the structure became loose [19].

3.2. Effect of reaction conditions on Pb^{2+} adsorption

3.2.1. Effect of REC/CS ratio on adsorption

The REC/CS composite sponge with different mass ratio of REC and CS was prepared. The absorption experiments were carried out with 50 mL, 200 mg L^{-1} of Pb^{2+} solutions at room temperature and the results are shown in Fig. 4. A maximum adsorption capacity was obtained with the mass ratio up to 1:3. Evidently, during the initial period, the addition of REC increased adsorption sites, the adsorption capacity increased. With further increasing REC amount, the adsorption capacity decreased dramatically, which was

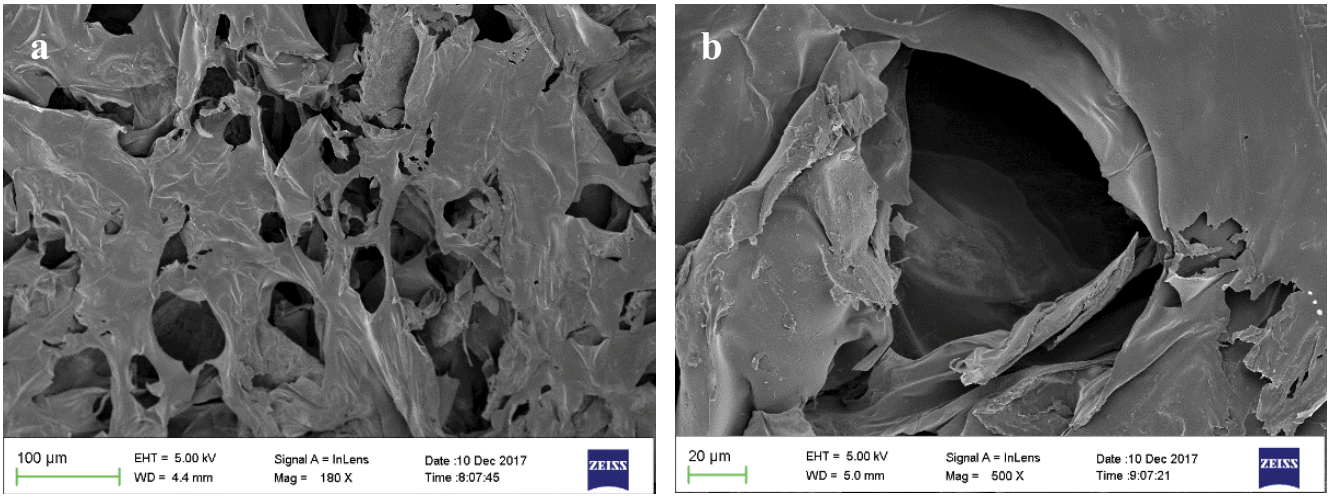

Fig. 1. SEM micrographs of REC/CS composite sponge with different magnification.

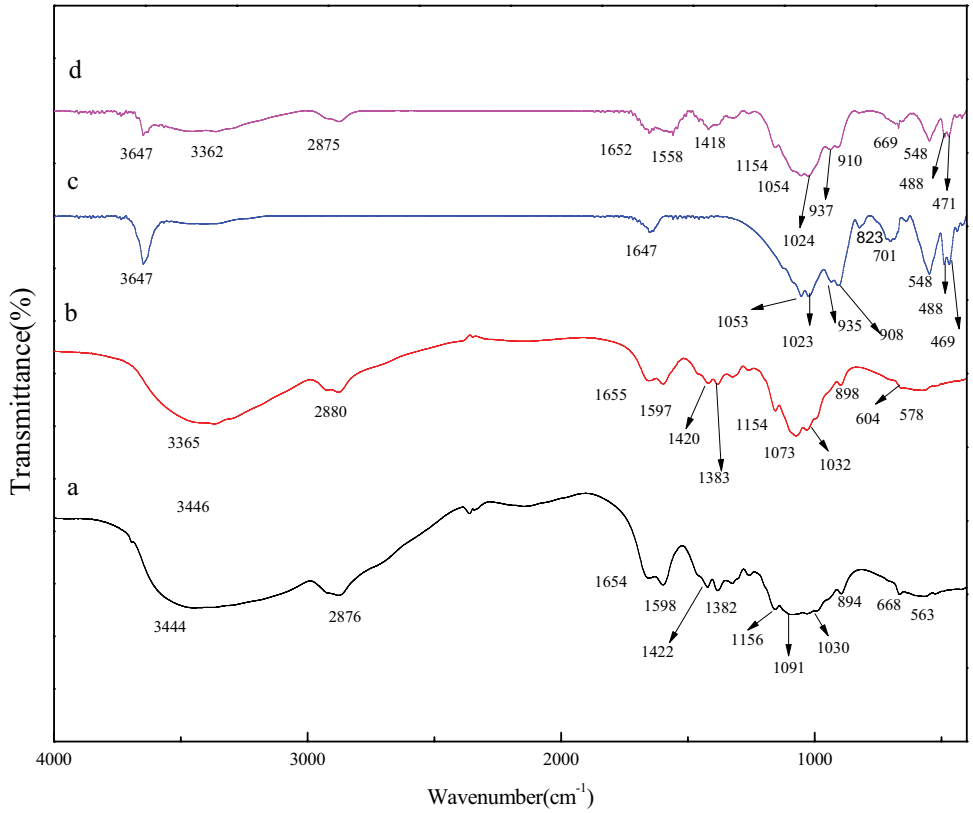

Fig. 2. FTIR spectra of CS (a), cross-linked CS sponge (b), REC powder (c) and REC/CS composite sponge (d).

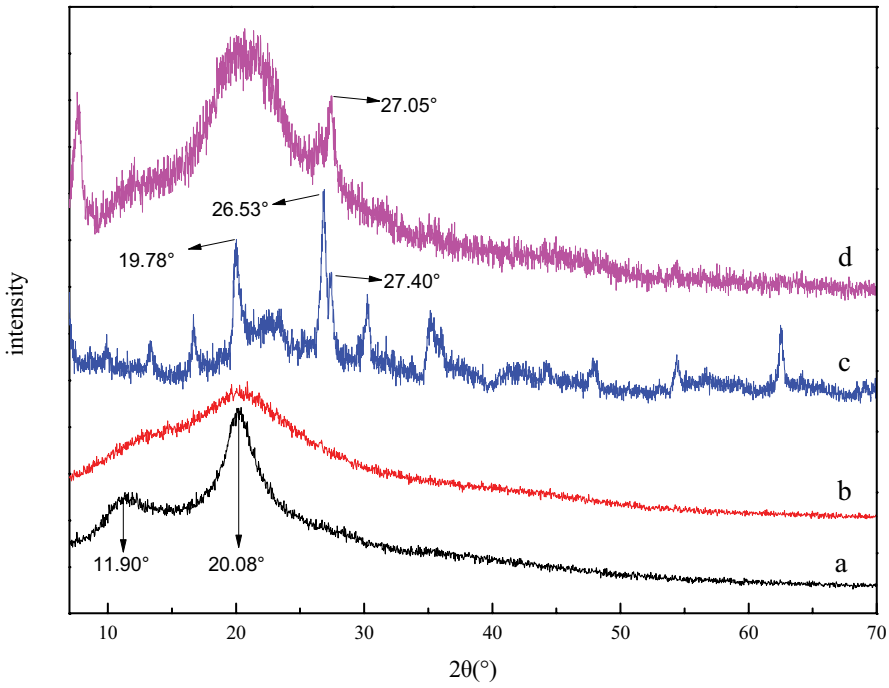

Fig. 3. XRD patterns of CS (a), cross-linked CS sponge (b), REC powder (c) and REC/CS composite sponge (d).

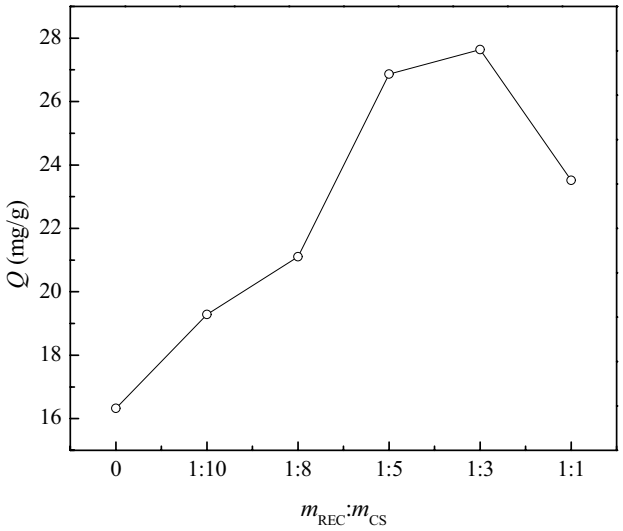

Fig. 4. Effect of REC/CS ratio on adsorption capacity.

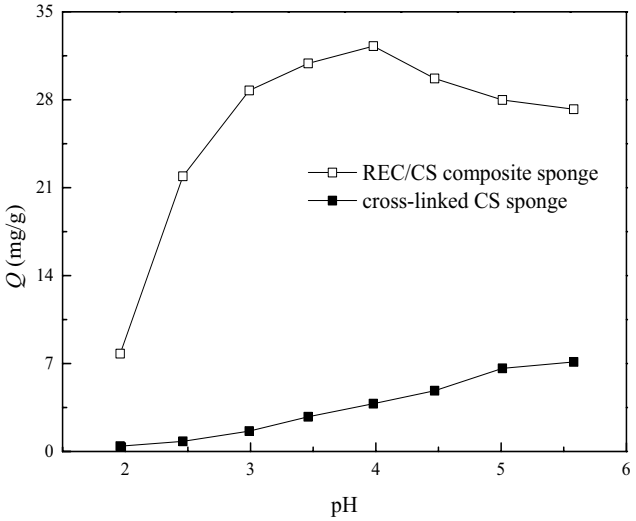

Fig. 5. Effect of pH on adsorption capacity.

attributed to the relative reduction of CS. CS was covered with REC, the adsorption capacity of REC is less than the adsorption capacity of CS.

3.2.2. Effect of pH on adsorption capacity

The pH is the most important factor affecting the adsorption process [20]. To investigate the effect of pH on the adsorption of Pb^{2+}, the experiment was carried out in 200 mg/L Pb^{2+} solutions, with pH values ranging from 2.0 to 5.5. The results could be seen in Fig. 5.

From Fig. 5, the adsorption capacity first increased and then slightly decreased with the increase of pH values. The adsorption capacity reached the optimum condition when pH was 4.0. At low pH, the concentration of H^+ in solution was relatively high. So most of $-NH_2$ had been protonated as Eq. (2), which might affect the target ions to approach the adsorption sites because the same charges repel each other [12]. In addition, ion exchange may be happened between the H^+ in solution and exchangeable cations in REC such as Na^+ thus competing with Pb^{2+}. These caused the low adsorption capacity at pH < 4. When the pH reached about 4.0, the hydrolysis reaction began to occur on aluminum in REC. Therefore, the generated precipitates would be attached on the surface of the materials, which influenced the contact between target ions and adsorption sites. Besides, the local concentration of H^+ would increase through hydrolysis reaction and decrease the adsorption capacity.

$$RNH_2 + H^+ \rightarrow RNH_3^+ \quad (2)$$

3.2.3. Effect of contact time

To investigate the effect of contact time on adsorption of Pb^{2+}, the static adsorption experiment was carried out in 200 mg/L Pb^{2+} solutions, and the concentration of residual Pb^{2+} was detected at different contact time and the result is shown in Fig. 6.

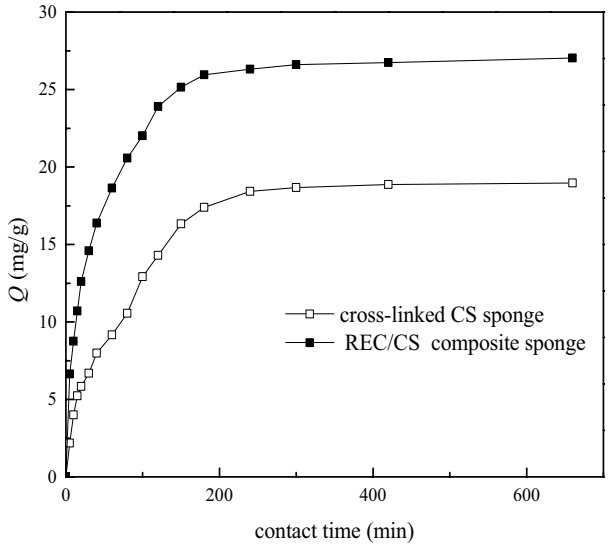

Fig. 6. Effect of contact time on adsorption capacity.

Totally, the adsorption capacity of Pb^{2+} onto the sponges increased rapidly within 120 min and then slowed down gradually until equilibrium reached. At the beginning, the available adsorption sites were sufficient, and the concentration of Pb^{2+} in solution was high. Therefore, the Pb^{2+} adsorption rate was fast due to the larger mass transfer force. Then, the vacant sites were occupied rapidly, and the concentration of Pb^{2+} in the residual solution declined as well, leading to the increase of the mass transfer resistance. So the adsorption rate was slower than that in the initial time, until the adsorption came to the dynamic equilibrium. According to the result, the adsorption process of cross-linked CS sponge and REC/CS composite sponge reached the equilibrium at about 240 and 180 min, respectively. The equilibrium adsorption capacity of cross-linked CS sponge and REC/CS composite sponge was 18.87 and 27.03 mg/g, respectively.

3.2.4. Effect of initial concentration on adsorption capacity

The effect of the initial Pb^{2+} concentration on adsorption capacity was studied by vibrating 100 mL various Pb^{2+} concentrations. As can be seen in Fig. 7, the adsorption capacity increased along with the increase of the initial concentration. The main reason was the quantity of vacant adsorption sites and the high concentration of Pb^{2+} in solution. But when the concentration was high enough, the adsorption sites were limited. So the increment of adsorption tended to be zero gradually, and the adsorption capacity reached the maximum. From the experimental data, the maximum adsorption capacity was obtained at Pb^{2+} = 600 mg/L, with 22.03 and 32.67 mg/g for cross-linked CS sponge and REC/CS composite sponge, respectively.

3.3. Adsorption kinetics

Three kinetic order models were studied to fit the experimental data: the pseudo-first-order, the pseudo-second-order, and the intra-particle diffusion model [21].

The pseudo-first-order model could be expressed by Eq. (3) [22].

$$\ln\left(Q_e - Q_t\right) = \ln Q_e - k_1 t \tag{3}$$

The pseudo-second-order model could be expressed by Eq. (4) and the initial adsorption rate h was expressed as Eq. (5) [23].

$$\frac{t}{Q_t} = \frac{1}{k_2 Q_e^2} + \frac{t}{Q_e} \tag{4}$$

$$h = k_2 Q_e^2 \tag{5}$$

The Weber–Morris intra-particle diffusion model was as follows:

$$Q_t = k_p t^{0.5} + C \tag{6}$$

In these equations, Q_e (mg/g) and Q_t (mg/g) represented the adsorption capacity at equilibrium and at time t, respectively. k_1 (min^{-1}), k_2 (g/(min mg)), and k_p (mg/g $min^{1/2}$) represented the constant of pseudo-first-order model, pseudo-second-order model, and internal diffusion rate, respectively. The C in Eq. (6) was the constant related to the thickness of the liquid film.

The fitting results are shown in Fig. 8, and the calculation parameters are shown in Table 1.

It could be seen that the adsorption process of cross-linked CS sponge and REC/CS composite sponge both fitted better with pseudo-second-order model than pseudo-first-order model, the correlation coefficient of pseudo-second-order model was closer to 1, and the calculated Q_e was closer to the experimental data. According to

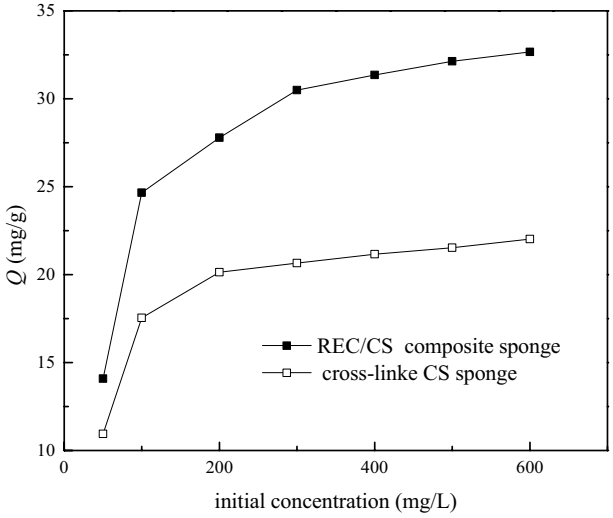

Fig. 7. Effect of initial concentration on adsorption capacity.

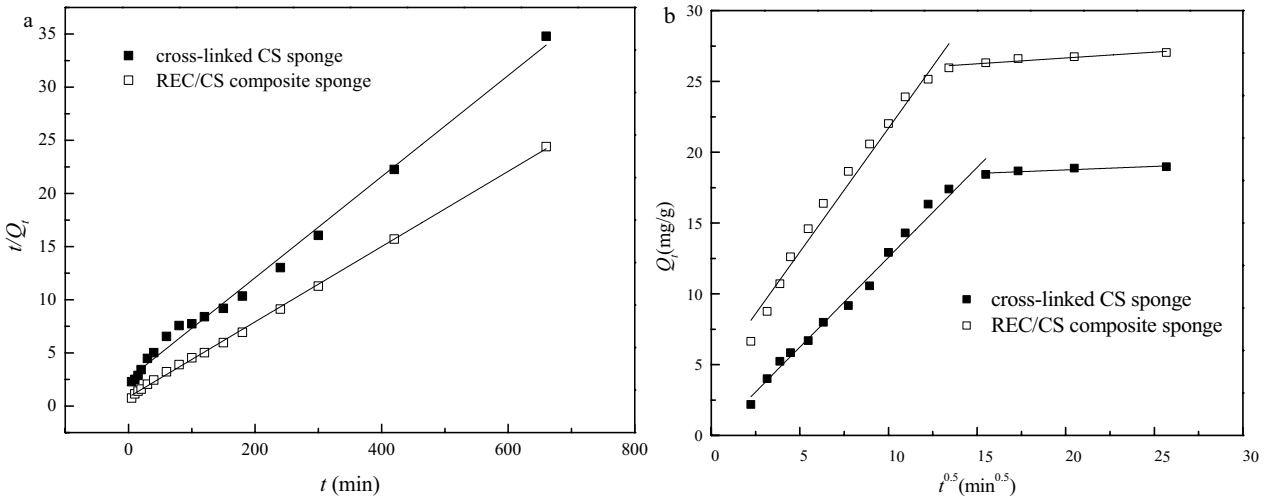

Fig. 8. Pseudo-second-order kinetics (a) and Weber–Morris intra-particle diffusion model (b) for Pb^{2+} sorption on REC/CS composite sponge.

Table 1, the theoretical equilibrium adsorption capacity of cross-linked CS sponge and REC/CS composite sponge calculated by pseudo-second-order model was 21.03 and 28.24 mg/g, respectively, and the initial adsorption rate was 0.3913 and 1.192 mg/(g min), respectively.

The adsorption process could be divided into two stages. As the *C* was not 0, the adsorption was determined by two steps, which was internal diffusion and liquid membrane diffusion. And the adsorption rate of the first step was faster than the second step, according to the value of k_{p1} and k_{p2}.

3.4. Isothermal adsorption

Adsorption isotherms are important for describing the interaction between adsorbent molecules and adsorbent surfaces. The Langmuir isotherm model assumes monolayer coverage of adsorbate on a homogeneous adsorbent surface. This model does not consider surface heterogeneity of the sorbent. It is assumed that adsorption would take place only on the special site of adsorbent. The Freundlich isotherm model is an empirical equation that describes the surface heterogeneity of the sorbent. It considers multilayer adsorption with a heterogeneous energetic distribution of active sites, accompanied by interactions of adsorbed molecules [24].

The Langmuir isotherm is expressed as:

$$\frac{C_e}{Q_e} = \frac{C_e}{Q_{\max}} + \frac{1}{Q_{\max} b} \tag{7}$$

where $Q_{\max}$ (mg/g) is the experimental maximum adsorption capacity, b is the Langmuir equilibrium constant, which is related to the affinity of binding sites in materials.

The Freundlich adsorption isotherm can be expressed as:

$$\log Q_e = \log k + \frac{1}{n} \log C_e \tag{8}$$

Both k and n in this formula represented the Freundlich isothermal adsorption constant. The value of k was related to adsorption capacity of adsorbent, while the n was related to adsorption intensity of adsorbent.

According to Fig. 9 and Table 2, Langmuir isothermal adsorption model could better fit the experimental data of adsorption. The correlation coefficients of the cross-linked CS sponge and REC/CS composite sponge for the Langmuir isothermal adsorption model were 0.9995 and 0.9993, respectively. And the correlation coefficients of the Freundlich isotherm model were 0.8167 and 0.9424, respectively. The result indicated that the adsorption of Pb^{2+} on the sponges were mainly monolayer adsorption and coexisted with other mechanisms [25]. Moreover, the theoretical maximum adsorption capacity of two kinds of materials was close to the experimental data. A comparative analysis on the removal of Pb^{2+} using various adsorbents is shown in Table 3. We observed that the $Q_{\max}$ value varied considerably for different adsorbents. In this study, the REC/CS composite sponge showed higher adsorption capacities compared with those of chitosan/clay composite. The nanocomposite and ion-imprinted polymers represented better performance.

3.5. Morphologies and structures of REC/CS composite sponge after adsorption of Pb^{2+}

The SEM-EDS and EDS mapping results of REC/CS composite sponge after adsorption are shown in Fig. 10. The porous structure of material was still complete after being soaked in solution for a long time. And the EDS result showed that the main element of material was C and O, and the content of Pb was ranked third after adsorption. The distribution of C and Pb elements was both uniform on the surface of the material, which also confirmed that REC/CS composite sponge had a certain adsorption ability for Pb^{2+}.

As it can be seen from Fig. 11, after adsorption of Pb^{2+}, the adsorption peak assigned to stretch vibration of N–H and O–H at 3,362 cm^{-1} shifted to 3,356 cm^{-1} as well as weakened, and the bending vibration adsorption peak of N–H at 1,595 cm^{-1} was weakened at the same time, which suggested the $–NH_2$ in CS still took part in the adsorption of Pb^{2+} onto REC/CS composite sponge. The adsorption band of stretching vibration in-plane of Si–O–Si enhanced and shifted from

Table 1
Adsorption parameters of kinetic models for Pb^{2+} sorption on REC/CS composite sponge

	Pseudo-first-order model				Pseudo-second-order model				
Parameter	k_1	Q_e	S_e	R^2	k_2	h	Q_e	S_e	R^2
	(min^{-1})	(mg/g)			(g/(mg min))	(mg/(g min))	(mg/g)		
CS sponge	1.309×10^{-2}	18.63	1.0322	0.9868	8.856×10^{-4}	0.3913	21.02	0.5239	0.9929
REC/CS sponge	1.166×10^{-2}	17.02	2.6753	0.9354	1.494×10^{-3}	1.192	28.24	0.0364	0.9991
Weber–Morris intra-particle diffusion model									
Parameter	k_{p1}	C_1	S_e	R^2	k_{p2}	C_2	S_e	R^2	
	(mg/g $min^{-1/2}$)				(mg/g $min^{-1/2}$)				
CS sponge	1.268	–0.105	0.2112	0.9914	0.0495	17.76	0.0137	0.7641	
REC/CS sponge	1.848	3.689	0.2999	0.9830	0.0823	25.01	0.0221	0.8717	

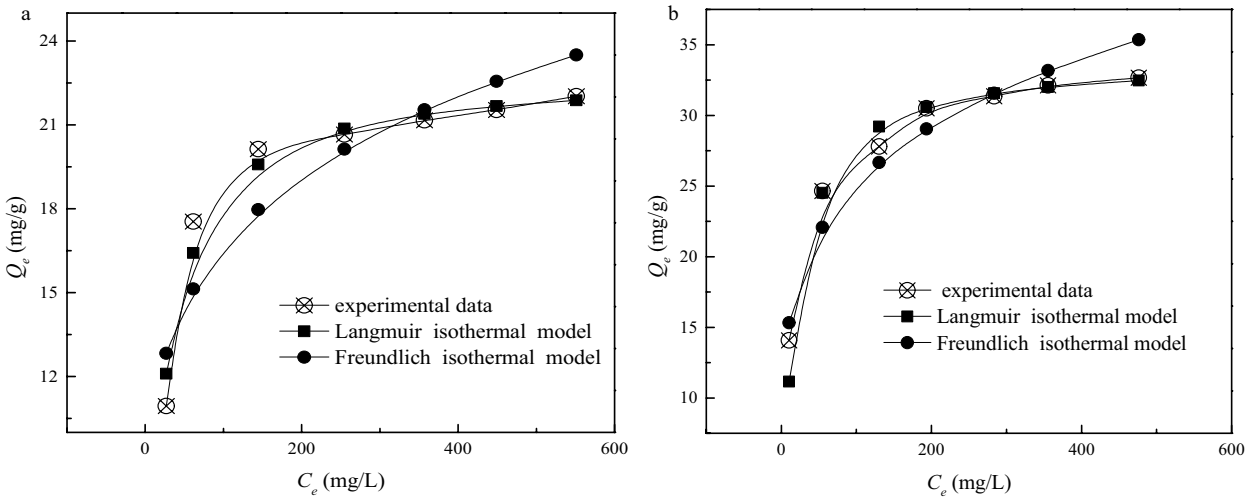

Fig. 9. Equilibrium adsorption of Pb^{2+} onto cross-linked CS sponge (a) and REC/CS composite sponge (b).

Table 2
Fitting result of adsorption parameter

	Langmuir adsorption model			Freundlich adsorption model		
Parameter	Q_{max} (mg/g)	b	R^2	$1/n$	k (L/g)	R^2
CS sponge	22.83	0.04168	0.9995	0.2008	6.618	0.8167
REC/CS sponge	33.90	0.04770	0.9993	0.2179	9.224	0.9424

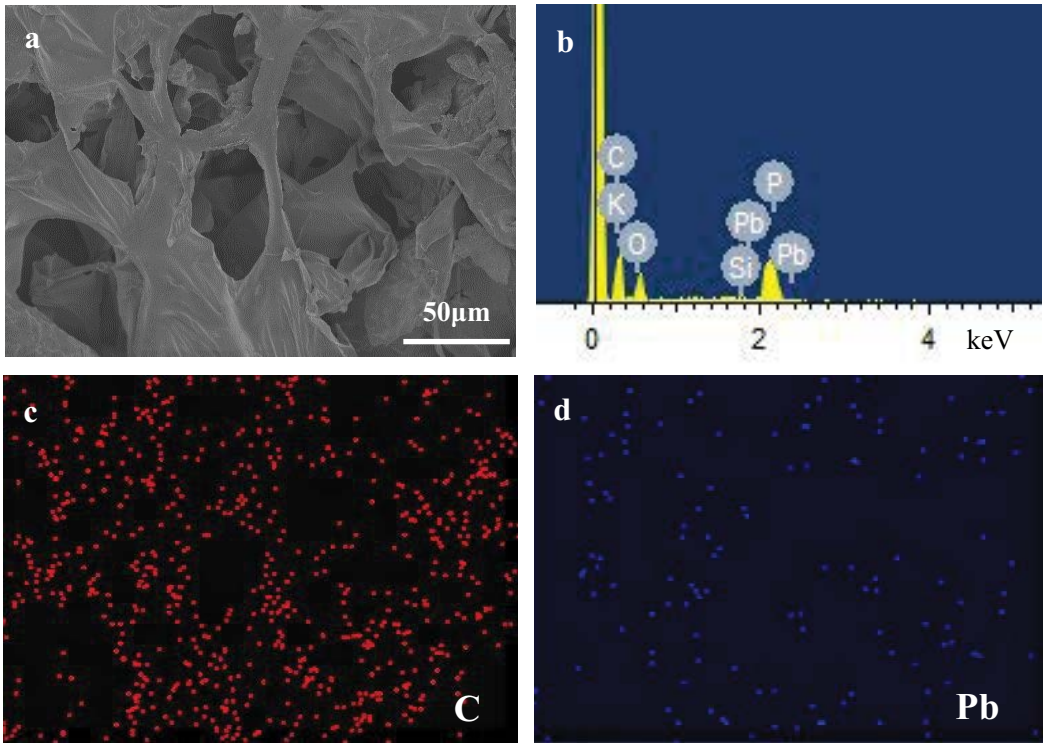

Fig. 10. (a) SEM of sample after adsorption of Pb^{2+}, (b) EDS spectrum, (c) C element distribution diagram, and (d) Pb element distribution diagram.

1,025 and 1,053 cm^{-1} to 1,020 and 1,049 cm^{-1}. The reason might be Pb^{2+} intercalating into the interlayer of REC, the binding force between the silica tetrahedron and the interlayer cations in the montmorillonite unit was weakened relatively. Meanwhile, the Si–O–Si in different silicon tetrahedron was much different due to ion exchanging.

It could be seen from Fig. 12 that after adsorption of Pb^{2+}, the crystallization characteristics of REC/CS composite sponge changed after adsorption of Pb^{2}, and the characteristic peaks weakened. Notably, there was a new peak appeared at 2θ = 27.42° belonging to Pb_2SiO_4 phase, because of the electrostatic attraction between Pb^{2+} and silicon oxy tetrahedron in REC.

Table 3
Comparison of the adsorption capacities (Q_{max}) of different adsorbents

Adsorbent	Q_{max} (mg/g)	Reference
Chitosan/rectorite composite sponge	33.9	This study
Chitosan-coated stone powder	17.2	[26]
Composite of hydroxyapatite and chitosan	3.1	[27]
Acid-activated clay	10.1	[28]
Alginate–bentonite	5.8	[29]
Lead ion-imprinted chitosan	83.2	[30]
Magnetic chitosan nanocomposite	121.9	[31]
Waterworks sludge waterworks sludge	20.4	[32]
Date pits activated carbon	101.3	[33]
Sodium dodecyl sulfate acrylamide Zr(IV) selenite	20.0	[34]

3.6. Recycling performance

In the present study, 0.01 M HCl solution was used to treat the sponges, which had adsorbed Pb^{2+} for the removal of the adsorbed ions. The mixture was agitated in a shaker at 120 rpm at room temperature for 4 h, and the adsorbents were washed repeatedly with distilled water until it became neutral. After that, they were used to re-adsorb the Pb^{2+} in aqueous solution. Repeat the experiment four times, and the changes of its adsorption capacity are shown in Fig. 13. The initial adsorption capacity of REC/CS composite sponge and cross-linked CS sponge is 25.95 and 17.39 mg/g, respectively. After five cycles, REC/CS composite sponge and cross-linked CS sponge exhibited 76.14% and 57.93% of maximum adsorption capacity, respectively. This result confirms that the REC/CS composite sponge has a good cyclic adsorption stability and regeneration ability.

4. Conclusion

The addition of REC not only improved the adsorption capacity of cross-linked CS sponge but also enhanced the intensity of cross-linked CS sponge. REC/CS composite sponge possess most effective Pb^{2+} adsorbing under the optimum pH value of 4, mREC:mCS = 1:3 and the crosslinking agent dosage of 0.8 mL. The equilibrium adsorption capacities of cross-linked CS sponge and REC/CS composite sponge were 18.87 and 27.03 mg/g, respectively. The adsorption of Pb^{2+} on cross-linked CS sponge was mainly attributed to the mating reaction of amino and hydroxyl groups on Pb^{2+}. Also, the ion exchange and electrostatic attraction may take part in the adsorption of REC/CS composite sponge. Both cross-linked CS sponge and REC/CS composite sponge exhibit a good fit with the

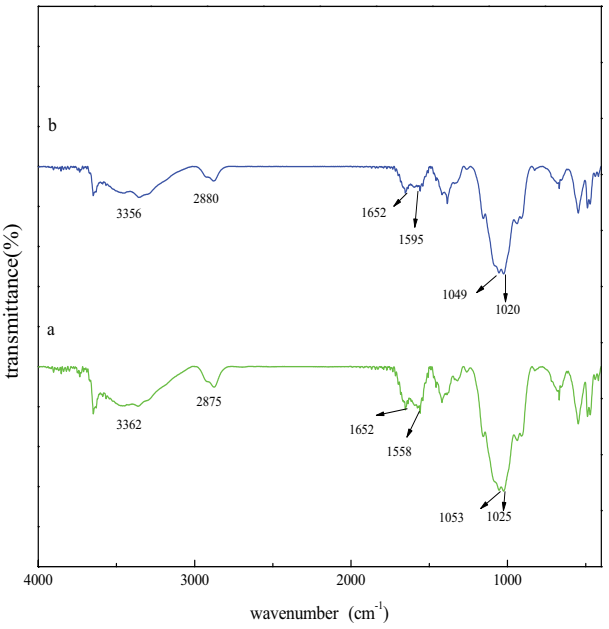

Fig. 11. FTIR spectra of samples after adsorption of Pb^{2+}. REC/CS composite sponge (a) before and (b) after adsorption.

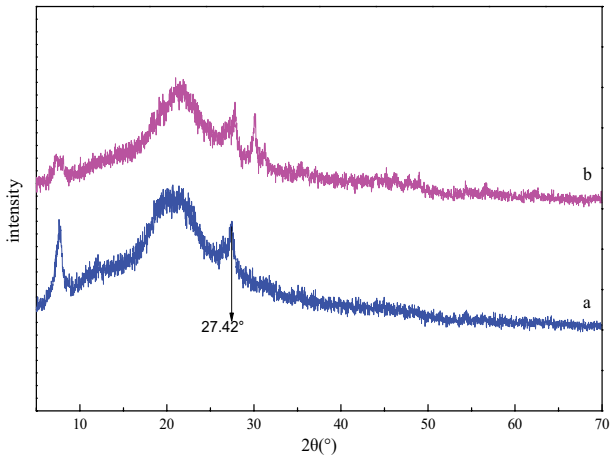

Fig. 12. XRD patterns of samples after adsorption of Pb^{2+}. REC/CS composite sponge (a) before and (b) after adsorption.

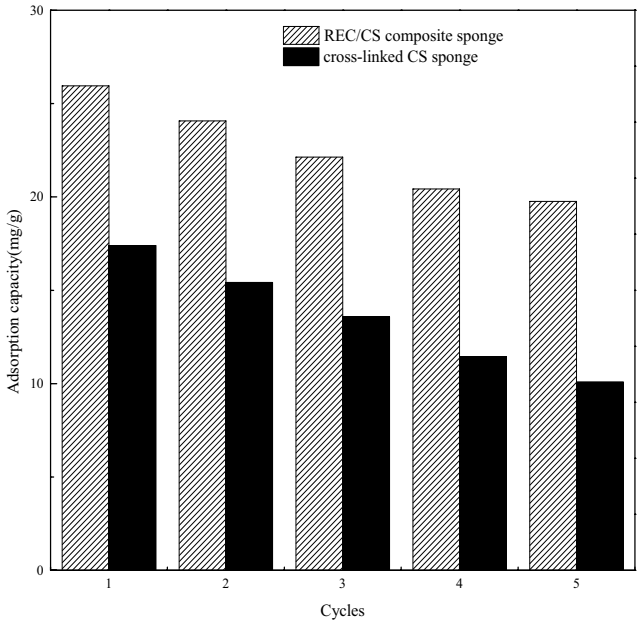

Fig. 13. Effect of regeneration times on adsorption capacity.

pseudo-second-order kinetic model and Langmuir isothermal adsorption model. REC/CS composite sponge has a better cyclic adsorption stability and regeneration ability than cross-linked CS sponge. Therefore, REC/CS composite sponge has promising applications in the removal of Pb^{2+} ions.

Acknowledgments

This work was supported by National Natural Science Foundation of China (50904047), the National Key Research and Development Program of China (2018YFB0605102), Science and Technology Department of Hubei Province (2019ZYYD060).

References

[1] C. Jin, X.Y. Zhang, J.N. Xin, G.F. Liu, J. Chen, G.M. Wu, T. Liu, J.W. Zhang, Z.W. Kong, Thiol-Ene synthesis of cysteine-functionalized lignin for the enhanced adsorption of Cu(II) and Pb(II), Ind. Eng. Chem., 57 (2018) 7872–7880.
[2] A.S. Özcould, Ö. Gök, A. Özcould, Adsorption of lead(II) ions onto 8-hydroxy quinoline-immobilized bentonite, J. Hazard. Mater., 161 (2019) 499–509.
[3] R.A. Jacques, E.C. Lima, S.L.P. Dias, A.C. Mazzocato, F.A. Pavan, Yellow passion-fruit shell as biosorbent to remove Cr(III) and Pb(II) from aqueous solution, Sep. Purif. Technol., 57 (2007) 193–198.
[4] M. Naushad, Z.A. ALOthman, Separation of toxic Pb^{2+} metal from aqueous solution using strongly acidic cation-exchange resin: analytical applications for the removal of metal ions from pharmaceutical formulation, Desal. Water Treat., 53 (2015) 2158–2166.
[5] J.M. Jacob, C. Karthik, R.G. Saratale, S.S. Kumar, D. Prabakar, K. Kadirvelu, A. Pugazhendhi, Biological approaches to tackle heavy metal pollution: a survey of literature, J. Environ. Manage., 217 (2018) 56–70.
[6] A.E. Burakov, E.V. Galunin, I.V. Burakova, A.E. Kucherova, S. Agarwal, A.G. Tkachev, V.K. Gupta, Adsorption of heavy metals on conventional and nanostructured materials for wastewater treatment purposes: a review, Ecotoxicol. Environ. Saf., 148 (2018) 702–712.
[7] C. Cheng, J. Wang, X. Yang, A. Li, C. Philippe, Adsorption of Ni(II) and Cd(II) from water by novel chelating sponge and the effect of alkali-earth metal ions on the adsorption, J. Hazard. Mater., 264 (2014) 332–341.
[8] L. Zhao, B. Yu, F. Xue, J. Xie, X. Zhang, R. Wu, R. Wang, Z. Hu, S. Yang, J. Luo, Facile hydrothermal preparation of recyclable S-doped graphene sponge for Cu^{2+}, adsorption, J. Hazard. Mater., 286 (2015) 449–456.
[9] Y. Liao, M. Wang, D.J. Chen, Preparation of polydopamine-modified graphene oxide/chitosan aerogel for uranium(VI) adsorption, Ind. Eng. Chem. Res., 57 (2018) 8472–8483.
[10] T. Feng, J. Wang, X. Shi, Removal of Cu^{2+} from aqueous solution by chitosan/rectorite nanocomposite microspheres, Desal. Water Treat., 52 (2014) 5883–5890.
[11] N.N. Wang, X.J. Xu, H.Y. Li, L.Z. Yuan, H.W. Yu, Enhanced selective adsorption of Pb(II) from aqueous solutions by one-pot synthesis of xanthate-modified chitosan sponge: behaviors and mechanisms, Ind. Eng. Chem. Res., 55 (2016) 12222–12231.
[12] L.X. Zeng, Y.F. Chen, Q.Y. Zhang, X.M. Guo, Y.N. Peng, H.J. Xiao, X.C. Chen, J.W. Luo, Adsorption of Cd(II), Cu(II) and Ni(II) ions by cross-linking chitosan/rectorite nano-hybrid composite microspheres, Carbohydr. Polym., 130 (2015) 333–343.
[13] X. Zhang, D.Y. Liu, K.N. Liu, Adsorption of modified rectorite on Pb^{2+} in waste liquor, Environ. Sci. Technol., 28 (2005) 16–17.
[14] Y.J. Lu, P.R. Chang, P.V. Zheng, X.F. Ma, Rectorite–TiO_2–Fe_3O_4 composites: assembly, characterization, adsorption and photodegradation, Chem. Eng. J., 255 (2014) 49–54.
[15] Y.J. Lu, P.R. Chang, P.V. Zheng, X.F. Ma, Porous 3D network rectorite/chitosan gels: preparation and adsorption properties, Appl. Clay Sci., 107 (2015) 21–27.
[16] X. Wang, B. Liu, J. Ren, C.F. Liu, X.H. Wang, J. Wu, R.C. Sun, Preparation and characterization of new quaternized carboxymethyl chitosan/rectorite nanocomposite, Compos. Sci. Technol., 70 (2010) 1161–1167.
[17] V. Nair, A. Panigrahy, R. Vinu, Development of novel chitosan–lignin composites for adsorption of dyes and metal ions from wastewater, Chem. Eng. J., 254 (2014) 491–502.
[18] J.W. Luo, G.C. Han, M.J. Xie, Z.R. Cai, X.Y. Wang, Quaternized chitosan/montmorillonite nanocomposite resin and its adsorption behavior, Iran. Chem. J., 24 (2015) 531–539.
[19] B. Liu, J.W. Luo, X.Y. Wang, J.X. Lu, H.B. Deng, R.C. Sun, Alginate/quaternized carboxymethyl chitosan/clay nanocomposite microspheres: preparation and drug-controlled release behavior, J. Biomater. Sci. Polym. Ed., 24 (2013) 589–605.
[20] T. Zhao, T. Feng, Application of modified chitosan microspheres for nitrate and phosphate adsorption from aqueous solution, RSC Adv., 6 (2016) 90878–90886.
[21] A. Kara, E. Demirbel, N. Tekin, B. Osman, N. Besirli, Magnetic vinylphenyl boronic acid microparticles for Cr(VI) adsorption: kinetic, isotherm and thermodynamic studies, J. Hazard. Mater., 286 (2015) 612–623.
[22] J. Febrianto, A.N. Kosasih, J. Sunarso, Y.H. Ju, N. Indraswati, S. Ismadji, Equilibrium and kinetic studies in adsorption of heavy metals using biosorbent: a summary of recent studies, J. Hazard. Mater., 162 (2009) 616–645.
[23] Y.S. Ho, G. Mckay, Pseudo-second order model for sorption processes, Process Biochem., 34 (1999) 451–465.
[24] T, Feng, S. Xiong, F. Zhang, Application of cross-linked porous chitosan films for Congo red adsorption from aqueous solution, Desal. Water Treat., 53 (2015) 1970–1976.
[25] P. Nanta, K. Kasemwong, W. Skolpap, Isotherm and kinetic modeling on superparamagnetic nanoparticles adsorption of polysaccharide, J. Environ. Chem. Eng., 6 (2018) 794–802.
[26] K. Jung, S. Oh, H. Bak, G.H. Song, H.T. Kim, Adsorption of arsenic and lead onto stone powder and chitosan-coated stone powder, Processes, 7 (2019) 599.
[27] N. Gupta, A.K. Kushwaha, M.C. Chattopadhyaya, Adsorptive removal of Pb^{2+}, Co^{2+} and Ni^{2+} by hydroxyapatite/chitosan composite from aqueous solution, J. Taiwan Inst. Chem. Eng., 43 (2012) 125–131.

[28] G. Resmi, S.G. Thampi, S. Chandrakaran, Removal of lead from wastewater by adsorption using acid-activated clay. Environ. Technol., 33 (2012) 291–297.
[29] T.W. Tzu, T. Tsuritani, K. Sato, Sorption of Pb(II), Cd(II), and Ni(II) toxic metal ions by alginate-bentonite, J. Environ. Prot., 4 (2013) 51–55.
[30] H. Wang, H. Shang, X. Sun, L. Hou, M. Wen, Y. Qiao, Preparation of thermo-sensitive surface ion-imprinted polymers based on multi-walled carbon nanotube composites for selective adsorption of lead(II) ion, Colloid Surf., A, 585 (2020) 124139.
[31] S. Shahraki, H.S. Delarami, Magnetic chitosan-(D-glucosimine methyl) benzaldehyde Schiff base for Pb^{2+} ion removal, experimental and theoretical methods, Carbohydr. Polym., 200 (2018) 211–220.
[32] A.A.H. Faisal, S.F.A. Al-Wakel, H.A. Assi, L.A. Naji, M. Naushad, Waterworks sludge-filter sand permeable reactive barrier for removal of toxic lead ions from contaminated groundwater, J. Water Process. Eng., 33 (2020) 101112.
[33] R. Krishnamoorthy, B. Govindan, F. Banat, V. Sagadevan, M. Purushothaman, P.L. Show, Date pits activated carbon for divalent lead ions removal, J. Biosci. Bioeng., 128 (2019) 88–97.
[34] M. Naushad, Surfactant assisted nano-composite cation exchanger: development, characterization and applications for the removal of toxic Pb^{2+} from aqueous medium, Chem. Eng. J., 235 (2014) 100–108.